Functional Architecture of RNA Polymerase I

Claus-D. Kuhn,[1] Sebastian R. Geiger,[1] Sonja Baumli,[1,4] Marco Gartmann,[1] Jochen Gerber,[2] Stefan Jennebach,[1] Thorsten Mielke,[3] Herbert Tschochner,[2] Roland Beckmann,[1] and Patrick Cramer[1,*]

[1]Gene Center Munich and Center for Integrated Protein Science CIPSM, Department of Chemistry and Biochemistry, Ludwig-Maximilians-Universität München, Feodor-Lynen-Str. 25, 81377 Munich, Germany
[2]Institut für Biochemie, Genetik und Mikrobiologie, Universität Regensburg, Universitätsstr. 31, 93053 Regensburg, Germany
[3]Ultrastrukturnetzwerk, Max Planck Institute for Molecular Genetics, Ihnestr. 63-73, 14195 Berlin, Germany
[4]Present address: Laboratory of Molecular Biophysics, Department of Biochemistry, University of Oxford, South Parks Road, Oxford, OX1 3QU, UK.
*Correspondence: cramer@LMB.uni-muenchen.de

SUMMARY

Synthesis of ribosomal RNA (rRNA) by RNA polymerase (Pol) I is the first step in ribosome biogenesis and a regulatory switch in eukaryotic cell growth. Here we report the 12 Å cryo-electron microscopic structure for the complete 14-subunit yeast Pol I, a homology model for the core enzyme, and the crystal structure of the subcomplex A14/43. In the resulting hybrid structure of Pol I, A14/43, the clamp, and the dock domain contribute to a unique surface interacting with promoter-specific initiation factors. The Pol I-specific subunits A49 and A34.5 form a heterodimer near the enzyme funnel that acts as a built-in elongation factor and is related to the Pol II-associated factor TFIIF. In contrast to Pol II, Pol I has a strong intrinsic 3′-RNA cleavage activity, which requires the C-terminal domain of subunit A12.2 and, apparently, enables ribosomal RNA proofreading and 3′-end trimming.

INTRODUCTION

The multisubunit RNA polymerases (Pol) I, II, and III catalyze DNA-dependent RNA synthesis in the eukaryotic nucleus. Whereas Pol II and Pol III synthesize mainly messenger and transfer RNAs, respectively, Pol I synthesizes ribosomal RNA (rRNA). Synthesis of rRNA is the first step in ribosome biogenesis and a focal point for the regulation of cell growth (Grummt, 2003; Moss et al., 2007). In yeast, Pol I activity accounts for up to 60% of all nuclear transcription, and the product rRNA accounts for up to 80% of all cellular RNA (Warner, 1999).

Pol I has a molecular weight of 590 kDa and comprises 14 subunits (Russell and Zomerdijk, 2006) (Table 1). Subunits Rpb5, Rpb6, Rpb8, Rpb10, and Rpb12 are identical in all three polymerases. The two large Pol I subunits A190 and A135 contain regions homologous to the Pol II subunits Rpb1 and Rpb2, respectively. Subunits AC40 and AC19 are identical in Pol I and Pol III, and homologous to the Pol II subunits Rpb3 and Rpb11, respectively. Subunits A14 and A43 form the heterodimer A14/43, which is distantly related to Rpb4/7 in Pol II and C17/25 in Pol III (Hu et al., 2002; Jasiak et al., 2006; Meka et al., 2003; Peyroche et al., 2002; Sadhale and Woychik, 1994; Siaut et al., 2003). For subunits A49 and A34.5, no counterparts in other polymerases have been found. Subunit A12.2 is homologous to subunit Rpb9 in Pol II and C11 in Pol III, but its C-terminal domain is also related to the Pol II transcript cleavage factor TFIIS.

To date most progress in structural studies of nuclear RNA polymerases has been made for Pol II, culminating in the refined atomic structures of the 10-subunit core (Cramer et al., 2001) and the complete enzyme (Armache et al., 2005). For Pol III, a 17 Å electron microscopy (EM) structure (Fernandez-Tornero et al., 2007) and a homology model for the core enzyme and the crystal structure of the C17/25 subcomplex are available (Jasiak et al., 2006) (for comparability, EM resolutions throughout this paper generally refer to a Fourier shell correlation (FSC) of 0.5). For Pol I, the overall shape and dimensions were first revealed by EM analysis of two-dimensional crystals (Schultz et al., 1993). Subsequent cryo-EM at 34 Å resolution visualized a stalk containing A14/43, and densities for A49 and A34.5 over the central cleft (Bischler et al., 2002; Peyroche et al., 2002). Later EM analysis with cryo-negative staining at 22 Å confirmed the stalk but not the location of A49 and A34.5 (De Carlo et al., 2003).

Here we integrate structural biology methods to establish the complete subunit architecture and domain organization of Pol I. In addition, we define functional roles for subunits A49, A34.5, and A12.2, and report an intrinsic RNA cleavage activity of Pol I. The results uncover conserved and specific structural and functional principles in eukaryotic RNA polymerases and enable a detailed structure-function analysis of rRNA transcription.

RESULTS AND DISCUSSION

Cryo-EM Structure of Pol I at 12 Å Resolution

To study the Pol I structure in detail, we established a large-scale purification protocol for the complete

Table 1. Pol I Subunits

Polymerase part	Pol I subunit	MW (kDa)	Corresponding Pol II subunit	Subunit type	Sequence identity[1] (%)	Conserved Pol II fold[2] (%)
Core	A190	186.4	Rpb1	homolog	22.3	47.8
	A135	135.7	Rpb2	homolog	26.0	62.1
	AC40	37.7	Rpb3	homolog	21.2	53.5
	AC19	16.2	Rpb11	homolog	17.6	77.5
	A12.2	13.7	Rpb9	homolog	19.2	35.2
	Rpb5 (ABC27)	25.1	Rpb5	common	100	100
	Rpb6 (ABC23)	17.9	Rpb6	common	100	100
	Rpb8 (ABC14.5)	16.5	Rpb8	common	100	100
	Rpb10 (ABC10β)	8.3	Rpb10	common	100	100
	Rpb12 (ABC10α)	7.7	Rpb12	common	100	100
Subcomplex A14/43	A14	14.6	Rpb4	counterpart	4.5	25.0[3]
	A43	36.2	Rpb7	counterpart	8.0	78.4[3]
Subcomplex A49/34.5	A49	46.7	RAP74[4]	specific	7.6	57.2
	A34.5	26.9	RAP30[4]	specific	8.3	80.5
Total	-	589.6	-	-	29.5	60.8

[1] Number of amino acid residues in the Pol I subunit that are identical in the corresponding Pol II subunit divided by the total number of residues in the Pol I subunit. For A49/34.5, number of amino acid residues in the TFIIF RAP74/30 dimerization module structure that are identical in the A49/34.5 model divided by the total number of residues in the RAP74/30 heterodimer structure (Gaiser et al., 2000).

[2] Number of amino acid residues in the Pol II core structure that have the same fold in the Pol I homology model divided by the total number of residues in the Pol II subunit.

[3] For A43, number of amino acid residues in the Rpb7 structure that have the same fold in the A43 structure divided by the total number of residues in the Rpb7 structure. For A14, number of amino acid residues in the Rpb4 structure that have the same fold in the A14 structure divided by the number of residues of the tip-associated domain of Rpb4 (residues 1–155, HRDC domain excluded).

[4] Predicted to be partially homologous to the TFIIF subunits RAP74 and RAP30. For details see text.

14-subunit endogenous enzyme from *S. cerevisiae* that relies on an initial precipitation step (Gerber et al., 2007; Milkereit et al., 1997; Tschochner, 1996) (Experimental Procedures). Pol I preparations were monodisperse, comprised all subunits in a stoichiometric manner, contained single particles according to EM with negative staining, and enabled collection of high-quality cryo-EM data (Figure 1). The cryo-EM reconstruction with 46,056 particles led to a map at 11.9 Å resolution (Experimental Procedures, Figures 1D and 1E).

The crystal structure of the 10-subunit Pol II core was placed into the EM map as a rigid body by fitting the 5 common subunits, which occupy equivalent positions on the polymerases' surfaces (Jasiak et al., 2006). A perfect fit of the common subunits confirmed the high quality of the map (Figures 2A and 2B). Many regions of the homologous subunits fitted the map equally well, but strong deviations were also observed, in particular at the polymerase clamp and foot (Cramer et al., 2001) (Figures 2D and 2E). The clamp had swung inwards, entirely closing off the cleft (Figures 1E and 1F). This is the predominant state of the enzyme under our EM conditions (Experimental Procedures).

Homology Model of the Pol I Core

To explain differences between the EM map and the Pol II core structure, we constructed a homology model for the Pol I core. Modeling was achieved as for the Pol III core (Jasiak et al., 2006), but was complicated by the weaker sequence conservation between Pol II and Pol I subunits (Table 1). We identified regions of conserved fold in cycles of sequence alignment, model construction, detection of incorrect internal contacts, realignment of the erroneous sequence stretches, and construction of an improved model (Figures 2C and S1, Experimental Procedures). In the Pol I core model, well-conserved regions cluster around the active site, and peripheral regions are divergent (Figure S1). However, some peripheral Pol I domains, such as the jaw and lobe, resemble in shape the Pol II domains, suggesting that their folds are conserved despite divergent sequences. The predicted conservation of Pol II folds is far less in Pol I (60.8% overall, Table 1)
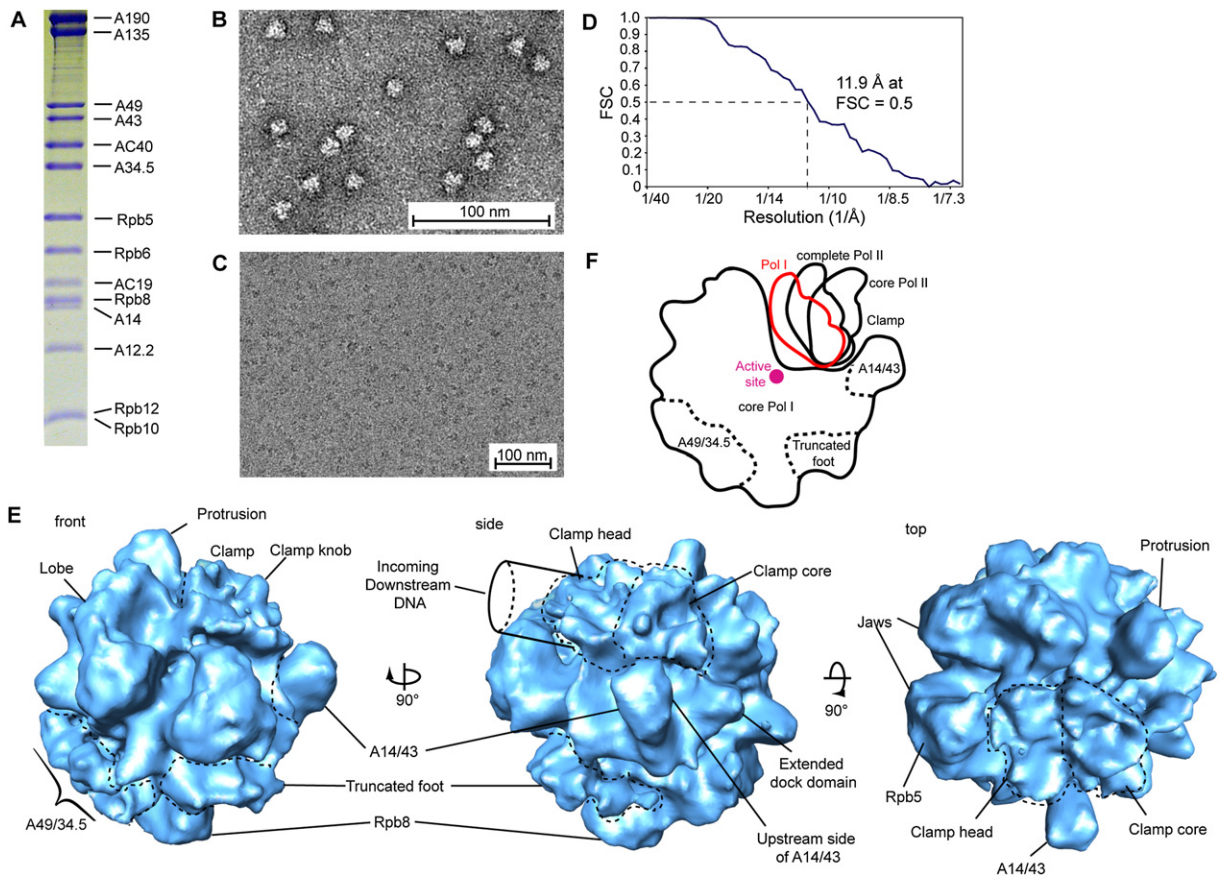
Figure 1. EM Reconstruction of Pol I
(A) SDS-PAGE analysis of purified yeast Pol I (Coomassie staining).
(B) EM image of negatively stained Pol I.
(C) EM image of Pol I variant △A49/34.5 under cryo conditions.
(D) Fourier shell correlation (FSC) function plot. Based on a cut-off value of FSC = 0.5, the resolution is 11.9 Å.
(E) Cryo-EM reconstruction of Pol I. Views and structural regions are named according to the Pol II structure (Cramer et al., 2001).
(F) Schematic representation of the clamp positions in Pol I, the complete 12-subunit Pol II (Armache et al., 2005), and the 10-subunit core Pol II (Cramer et al., 2001).

than in Pol III (83.4% for an 11-subunit model [Jasiak et al., 2006]).

Inspection of the EM map after placement of the core model confirmed the expected conservation of the active center, including the bridge helix, but also identified many structural features that create a Pol I-specific surface. The clamp shows two insertions near zinc site 7 ("clamp knob") and an extended, structurally different clamp head (Figures 1E and 2E). The dock domain shows density for a predicted (Chen and Hahn, 2003) Pol I-specific 14-residue extension (Figures 2C and 2E). In AC40, two surface elements differ from Rpb3 (Figures 2C and 2E). The foot domain has a divergent sequence, is 62 residues shorter, and has a different shape than in Pol II (Figures 2C and 2E). The jaw region contains 93 additional residues (Figure 2C), which are not conserved among fungi and lack EM density, showing they are mobile. A12.2 occupies the location of the Pol II core subunit Rpb9 and is thus a structural counterpart of Rpb9, not TFIIS (Figure 2B).

Crystal Structure of the A14/43 Subcomplex

After assigning EM densities to the Pol I core, a stalk-like density remained at the expected location for A14/43 that was much smaller than the structure of Rpb4/7 (Figures 1E, 2A, and S3). Since the weak sequence similarity between A14/43 and Rpb4/7 or C17/25 did not allow for homology modeling, we determined the crystal structure of A14/43 (Experimental Procedures). Partial proteolysis of a recombinant A14/43 heterodimer and bioinformatics revealed four mobile regions in A14/43 that were dispensable for dimerization (Figures 3A and S4). An A14/43 variant lacking the mobile regions crystallized and enabled structure determination at 3.1 Å resolution (Figure 3B and Table S1).

The overall structure of A14/43 resembles its counterparts Rpb4/7 (Armache et al., 2005), C17/25 (Jasiak et al., 2006), and the archaeal RpoF/E (Todone et al., 2001), except that A14 lacks the HRDC domain present in all counterparts (Figures 3B and S4). The N-terminal

tip domain of A43 shows RMS deviations in Cα atom positions of 2.2–2.5 Å, whereas the C-terminal OB domain is more divergent. A14 forms two helices that pack on the A43 tip domain (Figures 3B and S4).

Interaction of A14/43 with the Pol I Core
In Pol II, the Rpb4/7 complex interacts with the core enzyme via two loops, the A1-K1 loop, which forms a conserved contact of Rpb4/7-like subcomplexes with their cognate core enzymes, and the tip loop, which may confer specificity to the interaction in the different RNA polymerases (Armache et al., 2005; Jasiak et al., 2006). To dock the A14/43 structure into the EM map, we modeled the conserved contact between an invariant proline residue in the A1-K1 loop (P51 in A43, Figures 3B and 3D) and the common core subunit Rpb6 (Armache et al., 2005; Jasiak et al., 2006). The tip domain and the tip-associated domain of the A14/43 structure fitted well to the EM map, and the lack of an HRDC domain could in part explain the smaller EM density (Figure 3C). However, the peripheral OB domain of A43 was not revealed in the EM density (Figure 3C), suggesting a high degree of mobility. Consistently, the OB domain shows slightly higher B factors in the crystal structure, although it is involved in crystal contacts (Figure S5), and normal mode analysis of the Pol II crystal structure shows that the OB domain is the most flexible region of the enzyme (not shown). The A43 tip loop contains a specific ten-residue insertion that may confer specificity to the interaction between A14/43 and the Pol I core (Figure S4). The A43 tip loop is flexible in the crystal structure (Figures 3B and S4), but is likely folded upon binding to the Pol I core, as observed for Pol II (Armache et al., 2005).

Specific Interactions with Initiation Factors
Subunit A43 forms an essential bridge to the conserved Pol I initiation factor Rrn3 (Milkereit and Tschochner, 1998; Peyroche et al., 2000). Rrn3 was shown by EM to colocalize with A43 (Peyroche et al., 2000) and binds other initiation factors to recruit Pol I to the rDNA promoter. The A43-Rrn3 interaction is conserved in human (Yuan et al., 2002) and S. pombe (Imazawa et al., 2005). In a Pol I variant that is defective for Rrn3 interaction (rpa43-6 [Peyroche et al., 2000]), two out of three altered A43 residues map near conserved residues on the upstream surface of A14/43 (Figure 3D). Thus Rrn3 binds to A14/43 from the upstream side (Figure 1E). Additional Pol I-specific surfaces in the vicinity include the extended dock domain and the clamp knob, which together with A14/43 create a specific upstream face for Pol I initiation complex assembly (Figures 1 and 2).

Differential initiation factor interactions and promoter specificity of the three polymerases may generally result from differently structured dock domains, clamps, and Rpb4/7-like subcomplexes, which all constitute initiation factor binding sites. Rpb4/7 is required for Pol II initiation (Edwards et al., 1991). C17/25 binds to the Pol III initiation factor TFIIIB (Ferri et al., 2000), to the subcomplex C82/34/31 that bridges to TFIIIB (Bartholomew et al., 1993; Brun et al., 1997; Thuillier et al., 1995), and to the initiation factor TFIIIC (Hsieh et al., 1999). Since the surfaces, flexibility, and in vivo function of the HRDC domains differ in Rpb4/7 and C17/25 (Jasiak et al., 2006), the absence of an HRDC domain in A14/43 is likely functionally significant.

A49 and A34.5 Form a TFIIF-like Heterodimer Near the Funnel
After assigning EM densities to the Pol I core and A14/43, one additional large density remained on the enzyme surface that was assigned to the Pol I-specific subunits A49 and A34.5 (Figure 1E). To confirm this assignment, we dissociated subunits A49 and A34.5 from Pol I with the use of urea (Huet et al., 1975), purified the resulting 12-subunit variant Pol I ΔA49/34.5 (previously called Pol A* [Huet et al., 1975]), and solved its structure by cryo-EM at 25 Å resolution (Figures 4A and 4B; Experimental Procedures). The structure was similar to the complete Pol I, except that the density assigned to A49 and A34.5 was lacking (Figure 4B). In addition, there was a minor change in the clamp conformation, which however represents an average clamp position and is unlikely to result from the absence of A49/34.5 (Experimental Procedures). Density assigned to A49 and A34.5 is located near the enzyme funnel, the external domain 1, a conserved core loop with a Pol I-specific insertion (corresponding to loop α16-β20 of the Pol II pore domain), and A12.2. This is consistent with loss of A49 when Pol I is purified from A12.2 deletion strains (Van Mullem et al., 2002).

To investigate the structure and function of A49 and A34.5, we searched for weak homologies with HHpred (Soding et al., 2005). Local homologies were detected between A49 and RAP74, the large subunit of the Pol II-associated factor TFIIF, and between A34.5 and RAP30, the small TFIIF subunit (Figure S6 and Experimental Procedures). Consistently, the N-terminal regions of A49 and A34.5 were predicted to contain β strands consistent with the fold of the RAP74-RAP30 dimerization module (Gaiser et al., 2000), and hydrophobic core residues in this fold were predicted to be conserved (Figures 4C and S6). Consistent with these predictions, bacterial coexpression of A49 and A34.5 enabled isolation of a stoichiometric A49/34.5 heterodimer (Figure 4D and Experimental Procedures) and alanine point mutations in three different conserved hydrophobic residues in the dimerization interface (I12 and Y76 in A49, W54 in A34.5) abolished or strongly impaired A49/34.5 copurification (not shown). Thus, A49 and A34.5 form a stable TFIIF-like heterodimerization module.

Heterodimerization of A49 and A34.5 explains why the two subunits dissociate together from Pol I upon urea treatment (Huet et al., 1975), why Pol I purified from a yeast strain lacking the gene for A34.5 also lacks A49 (Gadal et al., 1997), and why two distantly related mammalian Pol I subunits bind each other (Yamamoto et al., 2004). It is also consistent with the observed continuous EM
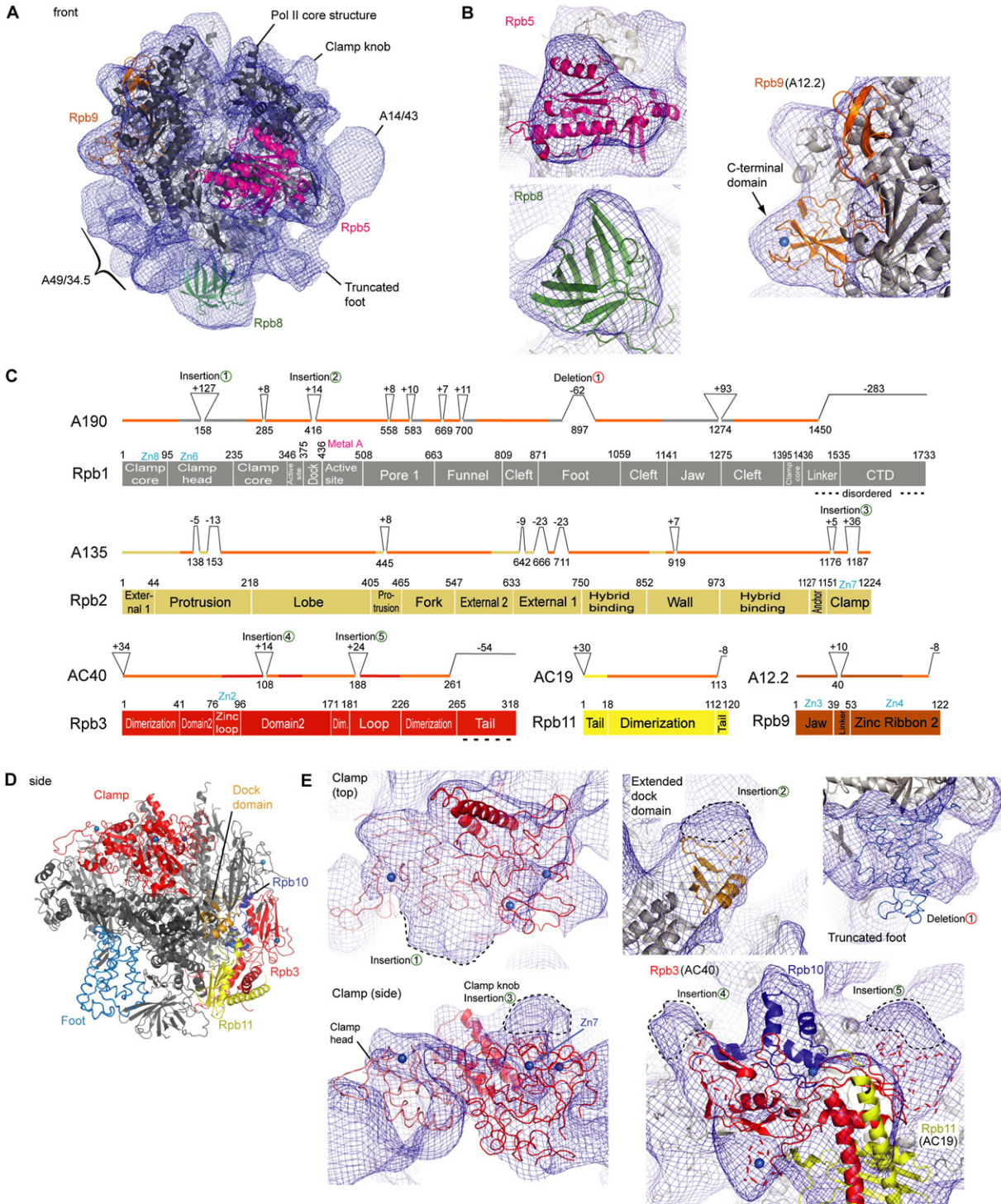
Figure 2. Model and EM Features of the Pol I Core

(A) Placement of the Pol II ten-subunit core structure (Armache et al., 2005) (gray) into the EM density (blue). The foot was deleted, and subunits Rpb5, Rpb8, and Rpb9 are highlighted in magenta, green, and orange, respectively. The clamp has been fitted as a separate rigid body.

(B) Fit of the common subunits Rpb5 and Rpb8 to the EM map, and density for the core subunit A12.2 (the Pol II homolog Rpb9 is shown as a ribbon model).

(C) Pol II structure-guided sequence alignment of the five Pol I subunits with homologs in Pol II (compare Table 1). The domain organization of Pol II subunits Rpb1, Rpb2, Rpb3, Rpb11, and Rpb9 is shown as diagrams (Cramer et al., 2001). Insertions and deletions exceeding five amino acid residues are indicated. Conserved folds are indicated by orange highlighting of the bar above the diagrams. For details see Figure S1.
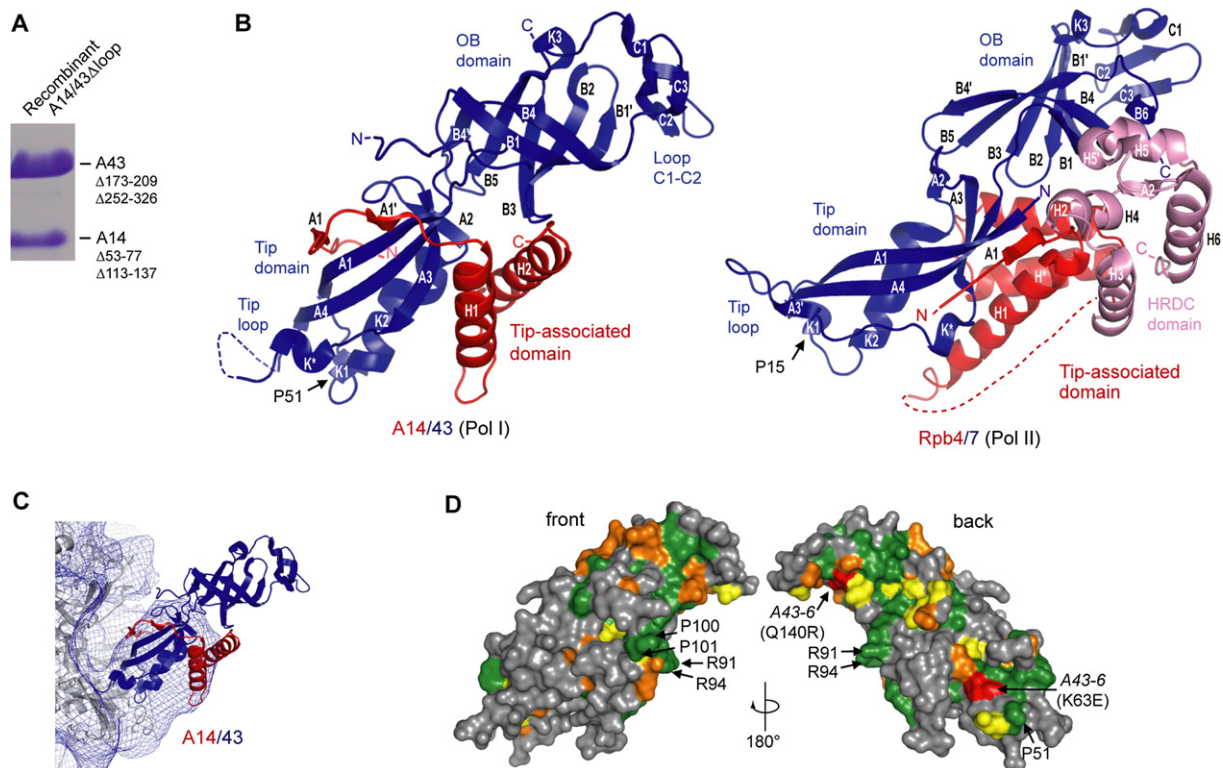
Figure 3. X-Ray Structure of the A14/43 Subcomplex

(A) SDS-PAGE analysis of purified yeast A14/43 △ loop used for crystallization (Experimental Procedures).

(B) Structures of yeast A14/43 (left) and Rpb4/7 (Armache et al., 2005) (right). A43 and Rpb7 are in blue and A14 and Rpb4 are in red, with the HRDC domain in light red. For details see Figure S4. The view is as in Figures 1E and 2A.

(C) Fit of the A14/43 structure into the Pol I EM density.

(D) Surface representation of the A14/43 complex. Residues conserved among eight selected *Saccharomycotinae* are colored in green, orange, and yellow, according to decreasing conservation (compare Figure S4). Residues affected by the *A43-6* mutations (Peyroche et al., 2000) are in red.

density, which reconciles previous EM data. Initial cryo-EM showed two separated densities over the cleft that were assigned to A49 and A34.5 (Bischler et al., 2002). EM at higher resolution did not confirm these densities but revealed a new additional density (De Carlo et al., 2003) that was close to the location of A49/34.5 found here. The location of A49 and A34.5 distant from the DNA-binding cleft explains why neither A49 nor A34.5 could be crosslinked to DNA in Pol I initiation complexes (Bric et al., 2004).

The location of A49/34.5 at the Pol I funnel deviates from that of TFIIF on Pol II as observed by cryo-EM (Chung et al., 2003) but is more consistent with protein-protein crosslinking that maps TFIIF to the polymerase lobe and outer surface near Rpb9 (Chen et al., 2007). Discrepancies in the location of A49/34.5 and TFIIF may be explained by different locations of a related dimerization module on the

two polymerases, or by the presence of additional, unrelated domains in both factors. Sequence analysis showed that A49/34.5 and TFIIF possibly have a counterpart in Pol III, the C37/53 heterodimer (not shown), which may occupy a similar location on the Pol III surface near the lobe and funnel (Fernandez-Tornero et al., 2007).

A49/34.5 Is a Built-In Elongation Factor
The apparent homology of the A49/34.5 heterodimer with the N-terminal regions of the two large TFIIF subunits suggested that A49/34.5 has elongation-stimulatory activity. This prediction is consistent with previous reports that deletion of A49 or A49 and A34.5 reduce Pol I activity (Huet et al., 1975; Liljelund et al., 1992), and that A34.5 genetically interacts with DNA topoisomerase I (Gadal et al., 1997). We therefore compared the complete Pol I with Pol I △A49/34.5 in an RNA extension assay using

(D) View of the core Pol II structure (Cramer et al., 2001) from the side, with domains depicted in (E) highlighted.

(E) Pol I-specific structural elements. Fitted Pol II elements are shown as ribbon models. Insertions and deletions explaining the EM density are named according to (C). The clamp head is in light red and the clamp core in red. The dock and foot domains are in beige and blue, respectively, and Rpb3, Rpb10, and Rpb11 are in red, dark blue, and in yellow, respectively. Zinc ions are depicted as marine spheres.
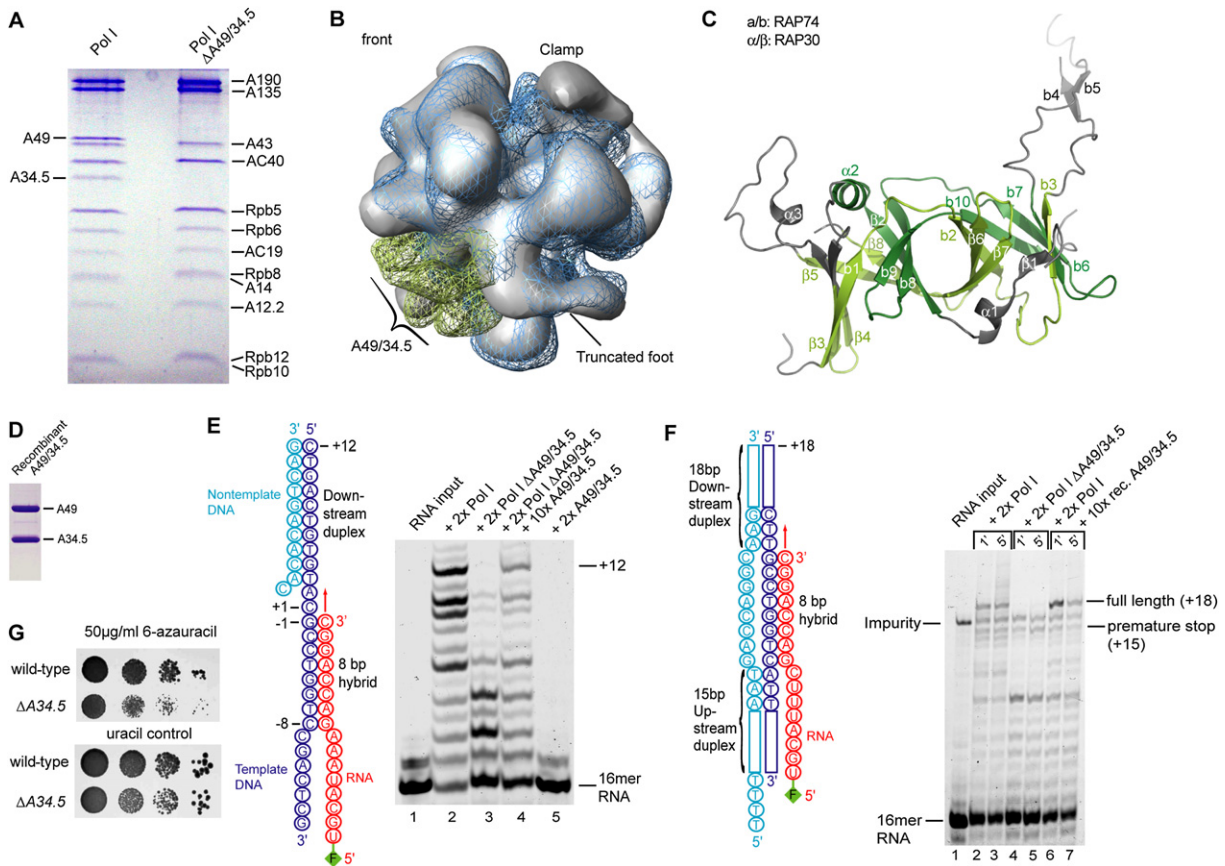
Figure 4. Structural and Functional Features of A49/34.5

(A) SDS-PAGE analysis of the variant Pol I △A49/34.5 (right), obtained by urea treatment of the complete Pol I (left).

(B) Overlay of EM structures of Pol I △A49/34.5 (silver surface) and the complete Pol I (blue). The density assigned to A49/34.5 is highlighted in green.

(C) Conservation of the TFIIF RAP74/30 dimerization module (Gaiser et al., 2000) in A49/34.5. Secondary structure elements aligned to RAP74/30 are highlighted in dark and light green, respectively. For details see Figure S5.

(D) SDS-PAGE analysis of recombinant A49/34.5 heterodimer.

(E) A49/34.5 shows elongation-stimulatory activity in RNA extension assays with a minimal nucleic-acid scaffold. The fluorescent label 6-carboxy-fluoresceine (FAM) on the RNA 5′ end is indicated. The times molar excess of added factors are indicated above the lanes. For lane 4, Pol I △A49/34.5 was complemented with a 5-fold molar excess of recombinant A49/34.5 for 10 min at 20°C prior to addition of the scaffold.

(F) Elongation assay as in (E) but with a complete complementary bubble (Kireeva et al., 2000).

(G) Deletion of the gene for A34.5 leads to a 6-azauracile-sensitive phenotype. From left to right 1:10 dilution series are shown. As a control, cells were spread onto SDC plates containing uracil.

a minimal DNA-RNA scaffold (Brueckner et al., 2007). The complete Pol I extended the RNA to the end of the template, whereas Pol I △A49/34.5 did not produce the run-off product (Figure 4E). Addition of recombinant A49/34.5 rescued the defect of Pol I △A49/34.5 and enabled elongation to the end of the template (Figure 4E, lane 4). We repeated the elongation experiments using a complete, complementary transcription bubble scaffold (Kireeva et al., 2000) (Figure 4F). The complete Pol I produced the run-off transcript (+18), whereas Pol I △A49/34.5 did not, but addition of recombinant A49/34.5 heterodimer restored run-off formation (Figure 4F). The defect was not due to differential binding of the polymerase variants to the scaffold, as it was also observed when the elongation complexes were covalently coupled to magnetic beads

and extensively washed before the reaction (not shown). Thus, A49/34.5 is required for normal elongation activity of Pol I in vitro.

To test whether A49/34.5 may have elongation-stimulatory function in vivo, we investigated if the growth phenotype of a yeast strain that lacked the gene for A34.5 (△A34.5) is affected when nucleotide supply was limited due to the presence of 6-azauracil (6AU). 6AU sensitivity is an indicator for Pol II-associated elongation factor function in vivo and recently also identified a Pol I mutant defective in rRNA elongation (Schneider et al., 2007). Whereas the wild-type and △A34.5 strains did not show a growth difference on normal media, the △A34.5 strain showed a mild slow-growth phenotype on 6AU-containing media (Figure 4G). This suggests that A49/34.5 is required
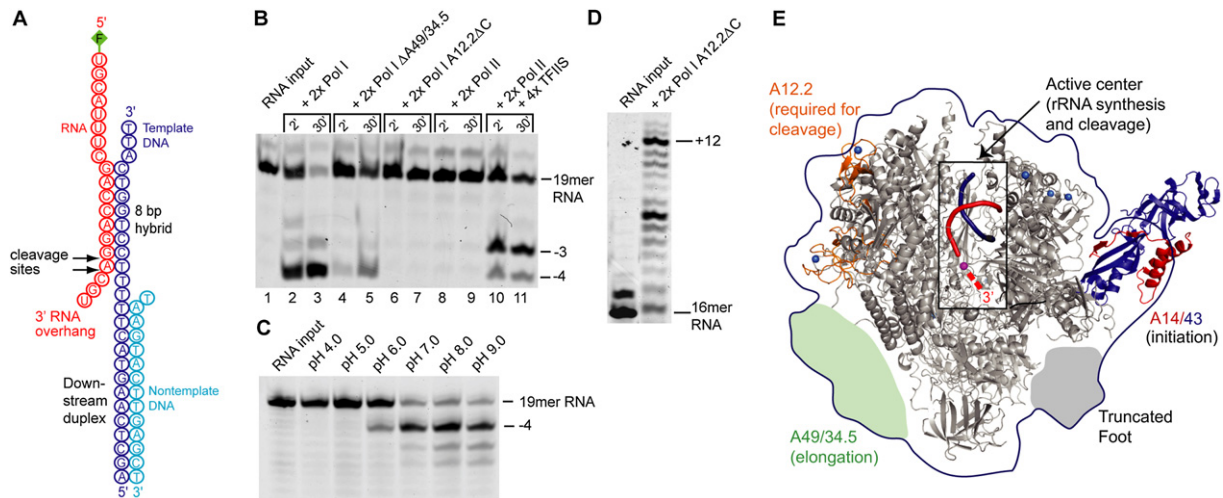
Figure 5. Intrinsic RNA Cleavage Activity and Functional Architecture of Pol I
(A) DNA-RNA hybrid scaffold used in cleavage assays.
(B) Comparison of RNA cleavage by Pol I variants with Pol II and the Pol II-TFIIS complex. Pol I mainly removed four nucleotides from the RNA, consistent with binding of the terminal hybrid base pair to the nucleotide insertion site (+1), extrusion of the RNA 3′ overhang into the polymerase pore and cleavage of the phosphodiester bond between nucleotides at positions −1 and +1 (Figure 5A). The Pol II-TFIIS complex removed three or four nucleotides, indicating that a mixture of complexes was present with the terminal hybrid base pair occupying either position −1 or +1.
(C) pH dependence of pol I cleavage activity.
(D) Elongation activity of the Pol I variant A12.2△C.
(E) Hybrid structure and functional architecture of Pol I. The EM envelope is shown as a blue line, the Pol I core ribbon model in gray with Rpb9 (A12.2) highlighted in orange, and the A14/43 crystal structure in red/blue. The window shows a cut-away view of the active center containing a modeled DNA-RNA hybrid. Red dashes indicate the RNA 3′ end extruded into the pore.

for normal RNA elongation by Pol I also in vivo. The elongation-stimulatory activity may be due to an allosteric effect or due to an extension from A49/34.5 into the active center, but we cannot distinguish between these possibilities with the available structural data.

Pol I Has Intrinsic RNA Cleavage Activity

The active site of Pol II exhibits weak 3′-RNA cleavage activity that is stimulated by TFIIS (Wind and Reines, 2000). For Pol I, a RNase H-like nuclease activity was initially described (Huet et al., 1976), but was later found to reside in a dissociable factor (Huet et al., 1977; Iborra et al., 1979; Labhart, 1997; Tschochner, 1996). To clarify whether Pol I possesses intrinsic RNA cleavage activity, we assembled a "backtracked" elongation complex from purified Pol I and a DNA-RNA scaffold that contained an RNA 3′ overhang (Figure 5A) (Experimental Procedures). Incubation of the backtracked complex with 8 mM magnesium ions led to efficient shortening of the RNA from the 3′-end (Figure 5B, lanes 1–3). In comparison, Pol II was unable to cleave the RNA under these conditions, but addition of TFIIS resulted in cleavage (Figure 5B, lanes 8–11). Thus, Pol I has a strong intrinsic RNA cleavage activity.

The intrinsic cleavage activity likely escaped detection previously since the nucleic-acid substrates used in published studies did not allow for the formation of a backtracked state, from which cleavage occurs. The previously

described dissociable factor (Huet et al., 1977; Iborra et al., 1979; Labhart, 1997; Tschochner, 1996) may not be required for cleavage per se, but may induce backtracking of Pol I, to create a state of the elongation complex that is prone to cleavage.

Pol I Cleavage Activity Requires A12.2

Additional cleavage assays showed that the Pol I variant △A49/34.5 cleaved RNA less efficiently than the complete Pol I (Figure 5B, lanes 4 and 5). Cleavage stimulation by A49/34.5 is consistent with an early investigation of an RNase H-like activity in Pol I-containing fractions (Huet et al., 1976). We also asked whether subunit A12.2 is required for cleavage, since its counterpart C11 is essential for cleavage activity of Pol III (Chedin et al., 1998; Whitehall et al., 1994). A Pol I variant lacking residues 79–125 of A12.2 (A12.2△C, Experimental Procedures) was totally inactive in RNA cleavage (Figure 5B, lanes 6 and 7), but bound the nucleic-acid scaffold in electrophoretic mobility shift assays (not shown) and retained elongation activity (Figure 5D). Consistent with a function specific for the A12.2 C-terminal domain, a truncation variant remains bound to Pol I and does not show a conditional growth defect (Van Mullem et al., 2002).

The A12.2 C-terminal domain shows homology to the TFIIS C-terminal domain that inserts into the Pol II pore to stimulate RNA cleavage (Kettenberger et al., 2003), but its location in Pol I corresponds to that of the Rpb9

C-terminal domain on Pol II (Figure 2B). Although the long linker between the A12.2 N- and C-terminal domains could in principle allow swinging of the C-terminal domain into the pore, our results suggest that the effect of A12.2 truncation on cleavage is due to an allosteric rearrangement in the Pol I active center. The conserved polymerase active site is capable of RNA cleavage in the absence of cleavage stimulatory factors, since free Pol II and the bacterial RNA polymerase can cleave RNA under mild alkaline conditions (Orlova et al., 1995; Weilbaecher et al., 2003). Consistently, the intrinsic cleavage activity of Pol I increased with increasing pH (Figure 5C). The structural basis of the effect of A12.2 truncation on RNA cleavage awaits the crystal structure of Pol I.

Possible Functions of the Cleavage Activity

Since A12.2 is required for transcription termination (Prescott et al., 2004), Pol I cleavage activity may be involved in a termination-coupled reaction. RNA cleavage could be required for rRNA 3′-terminal trimming, a Pol I-associated RNA processing event that intimately follows termination and involves cleavage of ten nucleotides from the pre-rRNA 3′ end (Kuhn and Grummt, 1989). Consistently, Pol II can form a binary complex with RNA and cleave RNA from the 3′ end in the presence of TFIIS Johnson and Chamberlin, 1994).

It is very likely that the intrinsic cleavage activity of Pol I also enables rRNA proofreading to increase transcriptional fidelity. Indeed, repetition of our cleavage assay with a scaffold that contains only a single mismatch at the RNA 3′ end, mimicking the situation after a misincorporation event, induced efficient RNA cleavage (not shown). For Pol III, the intrinsic cleavage activity was recently shown to enable proofreading in a manner dependent on the A12.2 homolog C11 (Alic et al., 2007), which is required for the intrinsic cleavage activity of Pol III (Chedin et al., 1998; Landrieux et al., 2006).

Conclusions

Here we analyzed the detailed functional architecture of Pol I by a combination of structural biology techniques and structure-based functional analysis (Figure 5E). A comparison with the Pol II system revealed Pol I-specific features that match the unique nature of rRNA transcription. First, the distinct structure of the Pol I upstream face allows for specific initiation-factor interactions and recruitment of Pol I to the rRNA promoter. Second, the built-in elongation-stimulatory Pol I-specific subcomplex A49/34.5 can explain the efficient and processive nature of rRNA transcription during cell growth. Third, the intrinsic RNA cleavage activity apparently enables rRNA 3′ trimming and proofreading, to prevent formation of erroneous rRNAs and catalytically deficient ribosomes. Finally, our results unravel structural and functional relationships between the three eukaryotic transcription machineries and form the basis for a detailed structure-function analysis of rRNA transcription and processing.

EXPERIMENTAL PROCEDURES

Pol I Preparation

The *S. cerevisiae* strain GPY2, carrying a pAS22 plasmid coding for HA- and hexahistidine-tagged A43 (Fath et al., 2000), was grown in a 200 L fermenter overnight at 30°C, and cells were harvested at an OD_{600} of 5-6. Cells (30% slurry) were lysed by bead beating in 400 mM ammonium sulfate, 60 mM $MgCl_2$, 150 mM HEPES pH 7.8, 30% glycerol, 5 mM DTT, 1 mM PMSF, 1 mM benzamidine, 200 μM pepstatin, and 60 μM leupeptin. After filtration, the lysate was cleared by centrifugation (30 min, 8000 g), and ultracentrifugation (90 min; 30,000 g). The supernatant was dialyzed overnight at 4°C against 50 mM potassium acetate (KOAc), 20 mM HEPES at pH 7.8, 1 mM $MgCl_2$, 10% glycerol, and 10 mM β-mercaptoethanol. After centrifugation, (1 hr; 18,500 g), the pellet was resuspended in 1.5 M KOAc, 1 mM $MgCl_2$, 10% glycerol, and 10 mM β-mercaptoethanol and incubated with 8 ml Nickel-NTA agarose for 4 hr at 4°C. Bound protein was washed with 5 column volumes of 300 mM KOAc, 1 mM $MgCl_2$, 10% glycerol, and 10 mM β-mercaptoethanol and eluted with the same buffer containing 100 mM imidazole. Eluted protein was bound to an anion exchange column (MonoQ 10/100 GL) and eluted with a gradient from 300 mM to 2 M KOAc. Pol I eluted at 1100 mM KOAc. Pol I was bound to a cation exchange column (MonoS 5/50 GL), and eluted at 490 mM KOAc, using a gradient from 200 mM to 2 M KOAc. Final purification over a Superose 6 HR 10/30 size-exclusion column equilibrated with 60 mM ammonium sulfate, 1 mM $MgCl_2$, 5 mM HEPES at pH 7.8, 10 μM $ZnCl_2$ and 5 mM DTT, resulted in 0.5 mg of pure polymerase from 350–400 g of cells. For further details see Gerber et al. (2007).

Cryo-EM Structure Determinations

Purified Pol I at 0.1 mg/ml was applied to carbon-coated holey grids (Quantifoil) in 60 mM ammonium sulfate, 1 mM $MgCl_2$, 5 mM HEPES at pH 7.8, 10 μM $ZnCl_2$, and 5 mM DTT. Micrographs were recorded under cryo low-dose conditions (20 electrons/$Å^2$) on a Tecnai G2 Polara electron microscope at 300 kV and digitized on a Heidelberg drum scanner with a pixel size of 1.23 Å on the object scale. Defocus values were determined with CTFFIND and SPIDER (Frank et al., 1996). Particles were picked with SIGNATURE (Chen and Grigorieff, 2007) followed by visual inspection. Data were processed with SPIDER (Frank et al., 1996). Initially 31,600 particles from 15 micrographs were aligned using as a reference a truncated version of the complete Pol II structure (Armache et al., 2005) filtered at 20 Å resolution. As a control for reference bias, the clamp, foot, and Rpb4/7 (except the Rpb7 tip domain) were deleted from the Pol II structure. During early refinement, density for the clamp, foot, and Pol I-specific parts appeared, indicating the process was bias free. When Rpb4/7 was included in the reference structure, the density for A14/43 was much smaller already after the first round of refinement, and when the C-terminal domain of Rpb9 was removed from the reference, density for the corresponding A12.2 domain reappeared at the same location.

Particles were sorted iteratively into two subsets according to different clamp conformations (Cramer et al., 2001; Penczek et al., 2006). Sorting resulted in 19,130 particles with a defined closed clamp conformation (class I) and 12,546 particles with apparently different open clamp conformations (class II) with 3D reconstructions at a resolution of about 17 Å. After addition of more particles and further sorting and refinement, the class I dataset comprised 46,056 particles and led to a reconstruction at 11.9 Å resolution (FSC = 0.5). Refinement of the class II volume to higher resolution was impaired. Amplitudes were corrected by Fourier filtering.

For cryo-EM structure determination of Pol I △A49/34.5, data processing was carried out as for the complete Pol I and was again bias free. Twenty-one thousand particles of high defocus values (>3 μm) were aligned with SPIDER using the same reference. Only spurious density fragments were observed in the region assigned to the two dissociated subunits. After convergent cycles of particle sorting

(Penczek et al., 2006), the remaining 12,000 particles were back-projected, resulting in a 25 Å density.

Modeling of the Pol I Core

Rpb4/7 was removed from the Pol II structure (Armache et al., 2005), and the five common subunits were retained. For subunits Rpb1, Rpb2, Rpb3, Rpb9, and Rpb11, sequence alignments with their Pol I homologs were obtained with CLUSTAL W (Thompson et al., 1994) and were used for initial homology modeling. Side chains in these four Pol II subunits were kept when identical in the homologs and otherwise replaced by the most common rotamer of the counterpart residues. Regions in Pol II subunits that were not present in Pol I subunits were deleted. The resulting ten-subunit model was inspected residue by residue and showed meaningful internal contacts in most regions. Several regions, however, showed disallowed contacts, indicating misalignment of the corresponding sequence stretches. Manual realignment of these weakly conserved stretches (Figure S1) led to a model with good internal packing.

A14/43 Preparation

The genes for A14 and A43 were cloned sequentially into vector pET28b (Novagen), resulting in a thrombin-cleavable N-terminal hexahistidine tag on A14. A ribosomal binding site was introduced before A43 to enable bicistronic expression. The deletion construct A14$_{\triangle 53-77 \triangle 113-137}$/43$_{\triangle 173-209 \triangle 252-326}$ (A14/43$\triangle$loop) was generated by PCR overlap extension (Higuchi et al., 1988). Only regions that were proteolytically sensitive and/or not predicted to form secondary structure elements were deleted. A14/43$\triangle$loop was expressed for 18 hr at 18°C in *E. coli* BL21 (DE3) RIL cells (Stratagene) in 4 L of LB medium (Maniatis et al., 1982). Cells were harvested by centrifugation, resuspended in 100 ml buffer A (100 mM NaCl, 20 mM Tris pH 8.0, 10 mM β-mercaptoethanol, 1 mM protease inhibitor mix: 1 mM PMSF, 1 mM benzamidine, 200 μM pepstatin, and 60 μM leupeptin) and lysed by sonication. After centrifugation, the supernatant was loaded onto a 3 ml Ni-NTA column equilibrated with buffer A. After washing, proteins were eluted with buffer A containing 100 mM imidazole. Eluted fractions were diluted 3-fold with buffer A lacking NaCl and incubated with thrombin (1 U protease/1 mg protein) for 16 hr at 4°C. A Mono Q 10/10 GL anion exchange column was equilibrated with buffer B (100 mM NaCl, 20 mM Tris pH 8.0, 5 mM DTT), and proteins were eluted with a linear gradient from 100 mM to 1 M NaCl. A14/43 eluted at 220 mM NaCl. After concentration, the sample was applied to a Superose 12 HR 10/300 gel filtration column (GE Healthcare) equilibrated with buffer B. Pooled peak fractions were concentrated to 10 mg/mL.

A14/43 Crystal Structure Determination

Crystals of A14/43$\triangle$loop were grown at 20°C in hanging drops, using 22% PEG 3350 and 240 mM potassium acetate as reservoir solution. Crystals were harvested in reservoir solution, cryo-protected by stepwise transfer to reservoir solution containing 7%–20% PEG 400, and flash cooled by plunging into liquid nitrogen. Selenomethionine-labeled protein was prepared as described (Budisa et al., 1995; Meinhart et al., 2003) and crystallized at 20°C with the use of microseeding and a reservoir solution of 18% PEG 3350 and 350 mM potassium acetate. Crystals reached a size of 250 μm × 120 μm × 80 μm and were cryo-preserved as above. A SAD experiment was performed at the Swiss Light Source (Table S1). Data were processed with XDS (Kabsch, 1993). Programs SHELXD/HKL2MAP (Pape and Schneider, 2004; Schneider and Sheldrick, 2002) detected nine selenium sites, which stemmed from three A14/43$\triangle$loop complexes in the asymmetric unit. SHARP (de La Fortelle and Bricogne, 1997) was used for refining heavy-atom positions, SAD phasing, and density modification. The model was built with COOT (Emsley and Cowtan, 2004) and refined with CNS (Brunger et al., 1998) to a free R factor of 28.3% (Table S1). Ninety-eight and a half percent of the residues fall in allowed

and additionally allowed regions of the Ramachandran plot, and no residues fall in disallowed regions (Laskowski et al., 1993).

Preparation of A49/34.5

The genes for A49 and A34.5 were cloned sequentially into vector pET28b (Novagen), introducing a C-terminal hexahistidine tag on A49 and a second ribosomal binding site for bicistronic expression. The two subunits were coexpressed for 18 hr at 18°C in *E. coli* BL21 (DE3) RIL cells (Stratagene) in 4 L of Luria broth medium. Cells were harvested by centrifugation, resuspended in 100 ml buffer C (300 mM NaCl, 50 mM Tris pH 7.5, 10 mM β-mercaptoethanol, and 1 mM protease inhibitor mix), and lysed by sonication. After centrifugation the supernatant was loaded onto a 3 ml Ni-NTA column equilibrated with buffer C. The column was washed stepwise with 15 ml of buffer C containing 1 M NaCl and 15 ml of buffer C containing 30 mM imidazole. The A49/34.5 heterodimer was eluted with buffer C containing 100 mM imidazole. Eluted fractions were diluted 3-fold with 50 mM Tris pH 7.5 and 10 mM β-mercaptoethanol. A MonoS cation exchange column was equilibrated with buffer D (100 mM NaCl, 50 mM Tris pH 7.5, 5 mM DTT), and proteins were eluted with a linear gradient of 18 column volumes from 100 mM to 1 M NaCl. A49/34.5 eluted at 280 mM NaCl. The sample was applied to a Superose 12 HR 10/300 gel filtration column (GE Healthcare) equilibrated with buffer D. Pooled peak fractions were concentrated to 10 mg/mL.

A49/34.5 Structure Prediction

The sequences of A49 and A34.5 were submitted to HHpred (Soding et al., 2005). As the hit with the highest score, HHpred predicted similarity of the A49 N-terminal residues 52–102 to the N-terminal residues 99–150 of human RAP74 (p value = 0.0023). For A34.5 the hit with the third highest score was a similarity between the A34.5 residues 50–65 and residues 15–30 of human RAP30 (p value = 0.0003). Inspection of the predicted secondary structure elements in A49 and A34.5 revealed a similar arrangement of strands as in the RAP74/RAP30 dimerization module crystal structure (Gaiser et al., 2000) (PDB 1F3U) except that strands β4 and β5 were apparently lacking in A49, and no secondary structure corresponding to strands β6 and β7 of RAP30 was predicted in A34.5. The few residues conserved between A49 and RAP74 and between A34.5 and RAP30 generally lie within the hydrophobic heterodimer interface (Figure S6).

Yeast Genetic Manipulations and 6AU Phenotyping

To disrupt the gene for A34.5, *His5+* from *S. pombe* (complementing *HIS4* from *S. cerevisiae*) was amplified from pFA6a-HiS4MX6 (Longtine et al., 1998) using PCR. *S. cerevisiae* strain GPY2 was transformed by the LiAc method, and positive clones were selected using –his plates and verified by colony PCR. For testing elongation activity, GPY2 and GPY2$\triangle$RPA34, both harboring the pRS416 plasmid, were spotted on SDC plates lacking uracil and containing 60 μg/ml 6AU. Growth was monitored after 2 to 3 days at 30°C. To generate a C-terminal deletion in *RPA12* ($\triangle$G79-N125), the gene was deleted in GPY2 as above, but using *KanMX* instead of *His5+* as genetic marker. The resulting strain GPY2 (*rpa12::KanMX*) was transformed with a plasmid (pRS413-*RPA12[1–78]*) coding for residues 1–78 in A12.2. Transformants (*rpa12::KanMX*(pRS413-*RPA12[1–78]*)) were selected on SD plates –his and screened by colony PCR. A positive clone (Pol I A12.2$\triangle$C) was grown to an optical density of ~3 in SDC medium lacking histidine, using a 20 L fermenter.

Preparation of Pol I Variants

Pol I $\triangle$A49/34.5 was prepared by dialyzing Pol I-containing fractions after cation-exchange chromatography overnight against 2 M urea, 50 mM ammonium sulfate, 1 mM magnesium chloride, 20 mM HEPES at pH 7.8, 10% glycerol, and 5 mM DTT. A49/34.5 was separated from Pol I $\triangle$A49/34.5 by subsequent anion-exchange chromatography, applying a gradient from 50 mM to 1 M ammonium sulfate (Mono Q 5/50 GL, GE Healthcare). Pol I $\triangle$A49/34.5 eluted at 250 mM ammonium

sulfate and was further purified by size-exclusion chromatography (Superose 6 HR10/300) with buffer E (100 mM ammonium sulfate, 1 mM $MgCl_2$, 20 mM HEPES at pH 7.8, 5% glycerol, 5 mM DTT). Pooled fractions were concentrated to 0.5 mg/ml. Pol I variant A12.2△C was purified as the complete Pol I, except that gel filtration was omitted and was concentrated to 0.5 mg/ml in buffer E.

RNA Extension Assays

Four picomoles of polymerase was incubated for 30 min at 20°C with 2 pmol of a preannealed minimal nucleic-acid scaffold (template DNA: 3′-GCTCAGCCTGGTCCGCATGTGTCAGTC-5′; nontemplate DNA: 5′-CACACAGTCAG-3′; RNA: 5′-FAM-UGCAUAAAGACCAGGC-3′). For RNA elongation, complexes were incubated in the presence of 1 mM NTPs at 28°C for 20 min in transcription buffer (60 mM ammonium sulfate, 20 mM HEPES at pH 7.6, 8 mM magnesium sulfate, 10 μM zinc chloride, 10% glycerol, and 10 mM DTT). Reactions were stopped by addition of an equal volume 2× loading buffer (8 M urea, 2× TBE) and incubation for 5 min at 95°C. The FAM-labeled RNA extension products were separated by denaturing gel electrophoresis (0.5 pmol RNA per lane, 0.4 mm 15%–20% polyacrylamide gels containing 8 M urea, 50°C–55°C) and visualized with a Typhoon 9400 phosphoimager (GE Healthcare). For RNA extension assays with a complementary bubble (Kireeva et al., 2000), 6 pmol Pol I or Pol I △A49/34.5 were incubated for 15 min at 20°C with 3 pmol of a preannealed template DNA-RNA scaffold (template DNA: 3′-TGCGCACCACGCTTACT GGTCCGTTCGCCTGTCCTCGACCA-5′; RNA: 5′-FAM-UGCAUUUCG ACCAGG C-3′), followed by incubation with a 5-fold molar excess of nontemplate DNA (15 pmol; 5′-TTTTTACGCGTGGTGCGAATGACC AGGCAAGCGGACAGGAGCTGGT-3′) for 15 min at 25°C. Complexes were incubated in the presence of 1 mM NTPs at 28°C for 1 and 5 min in transcription buffer. Reactions were stopped and analyzed by gel electrophoresis as above.

RNA Cleavage Assays

Complexes of polymerase variants were formed in transcription buffer with a nucleic-acid scaffold that comprised an RNA with a 6-FAM fluorescent label at its 5′ end and a three-nucleotide noncomplementary overhang at its 3′ end (template DNA: 3′-TTACTGGTCCTTTTTCATGA ACTCGA-5′; nontemplate DNA: 5′-TAAGTACTTGAGCT-3′; RNA: 5′-F AM-UGCAUUUCGACCAGGACGU-3′, overhanging nucleotides underlined). Samples were incubated in transcription buffer up to 30 min at 28°C, and reaction products were analyzed as above.

Figure Preparation

Figures were prepared with CHIMERA (Pettersen et al., 2004) and PYMOL (DeLano Scientific).

Supplemental Data

Supplemental Data include six figures, one table, and Supplemental References and can be found with this article online at http://www.cell.com/cgi/content/full/131/7/1260/DC1/.

REFERENCES

Alic, N., Ayoub, N., Landrieux, E., Favry, E., Baudouin-Cornu, P., Riva, M., and Carles, C. (2007). Selectivity and proofreading both contribute significantly to the fidelity of RNA polymerase III transcription. Proc. Natl. Acad. Sci. USA 104, 10400–10405.

Armache, K.-J., Mitterweger, S., Meinhart, A., and Cramer, P. (2005). Structures of complete RNA polymerase II and its subcomplex Rpb4/7. J. Biol. Chem. 280, 7131–7134.

Bartholomew, B., Durkovich, D., Kassavetis, G.A., and Geiduschek, E.P. (1993). Orientation and topography of RNA polymerase III in transcription complexes. Mol. Cell. Biol. 13, 942–952.

Bischler, N., Brino, L., Carles, C., Riva, M., Tschochner, H., Mallouh, V., and Schultz, P. (2002). Localization of the yeast RNA polymerase I-specific subunits. EMBO J. 21, 4136–4144.

Bric, A., Radebaugh, C.A., and Paule, M.R. (2004). Photocross-linking of the RNA polymerase I preinitiation and immediate postinitiation complexes: implications for promoter recruitment. J. Biol. Chem. 279, 31259–31267.

Brueckner, F., Hennecke, U., Carell, T., and Cramer, P. (2007). CPD damage recognition by transcribing RNA polymerase II. Science 315, 859–862.

Brun, I., Sentenac, A., and Werner, M. (1997). Dual role of the C34 subunit of RNA polymerase III in transcription initiation. EMBO J. 16, 5730–5741.

Brunger, A.T., Adams, P.D., Clore, G.M., DeLano, W.L., Gros, P., Grosse-Kunstleve, R.W., Jiang, J.S., Kuszewski, J., Nilges, M., Pannu, N.S., et al. (1998). Crystallography & NMR system: A new software suite for macromolecular structure determination. Acta Crystallogr. D Biol. Crystallogr. 54, 905–921.

Budisa, N., Steipe, B., Demange, P., Eckerskorn, C., Kellermann, J., and Huber, R. (1995). High-level biosynthetic substitution of methionine in proteins by its analogs 2-aminohexanoic acid, selenomethionine, telluromethionine and ethionine in Escherichia coli. Eur. J. Biochem. 230, 788–796.

Chedin, S., Riva, M., Schultz, P., Sentenac, A., and Carles, C. (1998). The RNA cleavage activity of RNA polymerase III is mediated by an essential TFIIS-like subunit and is important for transcription termination. Genes Dev. 12, 3857–3871.

Chen, H.-T., Warfield, L., and Hahn, S. (2007). The positions of TFIIF and TFIIE in the RNA polymerase II transcription initiation complex. Nat. Struct. Mol. Biol. 8, 696–703.

Chen, H.T., and Hahn, S. (2003). Binding of TFIIB to RNA polymerase II: Mapping the binding site for the TFIIB zinc ribbon domain within the preinitiation complex. Mol. Cell 12, 437–447.

Chen, J.Z., and Grigorieff, N. (2007). SIGNATURE: a single-particle selection system for molecular electron microscopy. J. Struct. Biol. 157, 168–173.

Chung, W.H., Craighead, J.L., Chang, W.H., Ezeokonkwo, C., Bareket-Samish, A., Kornberg, R.D., and Asturias, F.J. (2003). RNA

polymerase II/TFIIF structure and conserved organization of the initiation complex. Mol. Cell *12*, 1003–1013.

Cramer, P., Bushnell, D.A., and Kornberg, R.D. (2001). Structural basis of transcription: RNA polymerase II at 2.8 angstrom resolution. Science *292*, 1863–1876.

De Carlo, S., Carles, C., Riva, M., and Schultz, P. (2003). Cryo-negative staining reveals conformational flexibility within yeast RNA polymerase I. J. Mol. Biol. *329*, 891–902.

de La Fortelle, E., and Bricogne, G. (1997). Maximum-likelihood heavy-atom parameter refinement for multiple isomorphous replacement and multiwavelength anomalous diffraction methods. Methods Enzymol. *276*, 472–494.

Edwards, A.M., Kane, C.M., Young, R.A., and Kornberg, R.D. (1991). Two dissociable subunits of yeast RNA polymerase II stimulate the initiation of transcription at a promoter *in vitro*. J. Biol. Chem. *266*, 71–75.

Emsley, P., and Cowtan, K. (2004). Coot: model-building tools for molecular graphics. Acta Crystallogr. D Biol. Crystallogr. *60*, 2126–2132.

Fath, S., Milkereit, P., Podtelejnikov, A.V., Bischler, N., Schultz, P., Bier, M., Mann, M., and Tschochner, H. (2000). Association of yeast RNA polymerase I with a nucleolar substructure active in rRNA synthesis and processing. J. Cell Biol. *149*, 575–590.

Fernandez-Tornero, C., Bottcher, B., Riva, M., Carles, C., Steuerwald, U., Ruigrok, R.W., Sentenac, A., Muller, C.W., and Schoehn, G. (2007). Insights into transcription initiation and termination from the electron microscopy structure of yeast RNA polymerase III. Mol. Cell *25*, 813–823.

Ferri, M.L., Peyroche, G., Siaut, M., Lefebvre, O., Carles, C., Conesa, C., and Sentenac, A. (2000). A novel subunit of yeast RNA polymerase III interacts with the TFIIB- related domain of TFIIIB70. Mol. Cell. Biol. *20*, 488–495.

Frank, J., Radermacher, M., Penczek, P., Zhu, J., Li, Y., Ladjadj, M., and Leith, A. (1996). SPIDER and WEB: processing and visualization of images in 3D electron microscopy and related fields. J. Struct. Biol. *116*, 190–199.

Gadal, O., Mariotte-Labarre, S., Chedin, S., Quemeneur, E., Carles, C., Sentenac, A., and Thuriaux, P. (1997). A34.5, a nonessential component of yeast RNA polymerase I, cooperates with subunit A14 and DNA topoisomerase I to produce a functional rRNA synthesis machine. Mol. Cell. Biol. *17*, 1787–1795.

Gaiser, F., Tan, S., and Richmond, T.J. (2000). Novel dimerization fold of RAP30/RAP74 in human TFIIF at 1.7 A resolution. J. Mol. Biol. *302*, 1119–1127.

Gerber, J., Reiter, A., Steinbauer, R., Jakob, S., Kuhn, C.-D., Cramer, P., Griesenbeck, J., Milkereit, P., and Tschochner, H. (2007). Site-specific phosphorylation of yeast RNA polymerase I. Nucleic Acids Res., in press. Published online December 15, 2007. 10.1093/nar/gkm1093.

Grummt, I. (2003). Life on a planet of its own: regulation of RNA polymerase I transcription in the nucleolus. Genes Dev. *17*, 1691–1702.

Higuchi, H., Yoshioka, T., and Maruyama, K. (1988). Positioning of actin filaments and tension generation in skinned muscle fibres released after stretch beyond overlap of the actin and myosin filaments. J. Muscle Res. Cell Motil. *9*, 491–498.

Hsieh, Y.J., Kundu, T.K., Wang, Z., Kovelman, R., and Roeder, R.G. (1999). The TFIIIC90 subunit of TFIIIC interacts with multiple components of the RNA polymerase III machinery and contains a histone-specific acetyltransferase activity. Mol. Cell. Biol. *19*, 7697–7704.

Hu, P., Wu, S., Sun, Y., Yuan, C.C., Kobayashi, R., Myers, M.P., and Hernandez, N. (2002). Characterization of human RNA polymerase III identifies orthologues for Saccharomyces cerevisiae RNA polymerase III subunits. Mol. Cell. Biol. *22*, 8044–8055.

Huet, J., Buhler, J.M., Sentenac, A., and Fromageot, P. (1975). Dissociation of two polypeptide chains from yeast RNA polymerase A. Proc. Natl. Acad. Sci. USA *72*, 3034–3038.

Huet, J., Wyers, F., Buhler, J.M., Sentenac, A., and Fromageot, P. (1976). Association of RNase H activity with yeast RNA polymerase A. Nature *261*, 431–433.

Huet, J., Buhler, J.M., Sentenac, A., and Fromageot, P. (1977). Characterization of ribonuclease H activity associated yeast RNA polymerase A. J. Biol. Chem. *252*, 8848–8855.

Iborra, F., Huet, J., Breant, B., Sentenac, A., and Fromageot, P. (1979). Identification of two different RNase H activities associated with yeast RNA polymerase A. J. Biol. Chem. *254*, 10920–10924.

Imazawa, Y., Hisatake, K., Mitsuzawa, H., Matsumoto, M., Tsukui, T., Nakagawa, K., Nakadai, T., Shimada, M., Ishihama, A., and Nogi, Y. (2005). The fission yeast protein Ker1p is an ortholog of RNA polymerase I subunit A14 in Saccharomyces cerevisiae and is required for stable association of RRN3p and RPA21 in RNA polymerase I. J. Biol. Chem. *280*, 11467–11474.

Jasiak, A.J., Armache, K.J., Martens, B., Jansen, R.P., and Cramer, P. (2006). Structural biology of RNA polymerase III: subcomplex C17/25 X-ray structure and 11 subunit enzyme model. Mol. Cell *23*, 71–81.

Johnson, T.L., and Chamberlin, M.J. (1994). Complexes of yeast RNA polymerase II and RNA are substrates for TFIIS-induced RNA cleavage. Cell *77*, 217–224.

Kabsch, W. (1993). J. Appl. Cryst. *26*, 795–800.

Kettenberger, H., Armache, K.-J., and Cramer, P. (2003). Architecture of the RNA polymerase II-TFIIS complex and implications for mRNA cleavage. Cell *114*, 347–357.

Kireeva, M.L., Komissarova, N., Waugh, D.S., and Kashlev, M. (2000). The 8-nucleotide-long RNA:DNA hybrid is a primary stability determinant of the RNA polymerase II elongation complex. J. Biol. Chem. *275*, 6530–6536.

Kuhn, A., and Grummt, I. (1989). 3′-end formation of mouse pre-rRNA involves both transcription termination and a specific processing reaction. Genes Dev. *3*, 224–231.

Labhart, P. (1997). Transcript cleavage in an RNA polymerase I elongation complex. Evidence for a dissociable activity similar to but distinct from TFIIS. J. Biol. Chem. *272*, 9055–9061.

Landrieux, E., Alic, N., Ducrot, C., Acker, J., Riva, M., and Carles, C. (2006). A subcomplex of RNA polymerase III subunits involved in transcription termination and reinitiation. EMBO J. *25*, 118–128.

Laskowski, R.A., MacArthur, M.W., Moss, D.S., and Thornton, J.M. (1993). PROCHECK: a program to check the stereochemical quality of protein structures. J. Appl. Cryst. *26*, 283–291.

Liljelund, P., Mariotte, S., Buhler, J.M., and Sentenac, A. (1992). Characterization and mutagenesis of the gene encoding the A49 subunit of RNA polymerase A in Saccharomyces cerevisiae. Proc. Natl. Acad. Sci. USA *89*, 9302–9305.

Longtine, M.S., McKenzie, A., 3rd, Demarini, D.J., Shah, N.G., Wach, A., Brachat, A., Philippsen, P., and Pringle, J.R. (1998). Additional modules for versatile and economical PCR-based gene deletion and modification in Saccharomyces cerevisiae. Yeast *14*, 953–961.

Maniatis, T., Fritsch, E.F., and Sambrook, J. (1982). Molecular Cloning, a Laboratory Manual (Cold Spring Harbor, N.Y.: Cold Spring Harbor Laboratory).

Meinhart, A., Blobel, J., and Cramer, P. (2003). An extended winged helix domain in general transcription factor E/IIEalpha. J. Biol. Chem. *278*, 48267–48274.

Meka, H., Daoust, G., Arnvig, K.B., Werner, F., Brick, P., and Onesti, S. (2003). Structural and functional homology between the RNAP(I) subunits A14/A43 and the archaeal RNAP subunits E/F. Nucleic Acids Res. *31*, 4391–4400.

Milkereit, P., and Tschochner, H. (1998). A specialized form of RNA polymerase I, essential for initiation and growth-dependent regulation of rRNA synthesis, is disrupted during transcription. EMBO J. *17*, 3692–3703.

Milkereit, P., Schultz, P., and Tschochner, H. (1997). Resolution of RNA polymerase I into dimers and monomers and their function in transcription. Biol. Chem. *378*, 1433–1443.

Moss, T., Langlois, F., Gagnon-Kugler, T., and Stefanovsky, V. (2007). A housekeeper with power of attorney: the rRNA genes in ribosome biogenesis. Cell. Mol. Life Sci. *64*, 29–49.

Orlova, M., Newlands, J., Das, A., Goldfarb, A., and Borukhov, S. (1995). Intrinsic transcript cleavage activity of RNA polymerase. Proc. Natl. Acad. Sci. USA *92*, 4596–4600.

Pape, T., and Schneider, T.R. (2004). HKL2MAP: a graphical user interface for phasing with SHELX programs. Acta Crystallogr. D Biol. Crystallogr. *37*, 843–844.

Penczek, P.A., Frank, J., and Spahn, C.M. (2006). A method of focused classification, based on the bootstrap 3D variance analysis, and its application to EF-G-dependent translocation. J. Struct. Biol. *154*, 184–194.

Pettersen, E.F., Goddard, T.D., Huang, C.C., Couch, G.S., Greenblatt, D.M., Meng, E.C., and Ferrin, T.E. (2004). UCSF Chimera-a visualization system for exploratory research and analysis. J. Comput. Chem. *25*, 1605–1612.

Peyroche, G., Levillain, E., Siaut, M., Callebaut, I., Schultz, P., Sentenac, A., Riva, M., and Carles, C. (2002). The A14–A43 heterodimer subunit in yeast RNA pol I and their relationship to Rpb4-Rpb7 pol II subunits. Proc. Natl. Acad. Sci. USA *99*, 14670–14675.

Peyroche, G., Milkereit, P., Bischler, N., Tschochner, H., Schultz, P., Sentenac, A., Carles, C., and Riva, M. (2000). The recruitment of RNA polymerase I on rDNA is mediated by the interaction of the A43 subunit with RRN3. EMBO J. *19*, 5473–5482.

Prescott, E.M., Osheim, Y.N., Jones, H.S., Alen, C.M., Roan, J.G., Reeder, R.H., Beyer, A.L., and Proudfoot, N.J. (2004). Transcriptional termination by RNA polymerase I requires the small subunit Rpa12p. Proc. Natl. Acad. Sci. USA *101*, 6068–6073.

Russell, J., and Zomerdijk, J.C. (2006). The RNA polymerase I transcription machinery. Biochem. Soc. Symp. *73*, 203–216.

Sadhale, P.P., and Woychik, N.A. (1994). C25, an essential RNA polymerase III subunit related to the RNA polymerase II subunit RPB7. Mol. Cell. Biol. *14*, 6164–6170.

Schneider, D.A., Michel, A., Sikes, M.L., Vu, L., Dodd, J.A., Salgia, S., Osheim, Y.N., Beyer, A.L., and Nomura, M. (2007). Transcription elongation by RNA polymerase I is linked to efficient rRNA processing and ribosome assembly. Mol. Cell *26*, 217–229.

Schneider, T.R., and Sheldrick, G.M. (2002). Substructure solution with SHELXD. Acta Crystallogr. D Biol. Crystallogr. *58*, 1772–1779.

Schultz, P., Celia, H., Riva, M., Sentenac, A., and Oudet, P. (1993). Three-dimensional model of yeast RNA polymerase I determined by electron microscopy of two-dimensional crystals. EMBO J. *12*, 2601–2607.

Siaut, M., Zaros, C., Levivier, E., Ferri, M.L., Court, M., Werner, M., Callebaut, I., Thuriaux, P., Sentenac, A., and Conesa, C. (2003). An Rpb4/Rpb7-like complex in yeast RNA polymerase III contains the orthologue of mammalian CGRP-RCP. Mol. Cell. Biol. *23*, 195–205.

Soding, J., Biegert, A., and Lupas, A.N. (2005). The HHpred interactive server for protein homology detection and structure prediction. Nucleic Acids Res. *33*, W244–W248.

Thompson, J.D., Higgins, D.G., and Gibson, T.J. (1994). CLUSTAL W: improving the sensibility of progressive multiple sequence alignment through sequence weighing, positions-specific gap penalties and weight matrix choice. Nucleic Acids Res. *22*, 4673–4680.

Thuillier, V., Stettler, S., Sentenac, A., Thuriaux, P., and Werner, M. (1995). A mutation in the C31 subunit of Saccharomyces cerevisiae RNA polymerase III affects transcription initiation. EMBO J. *14*, 351–359.

Todone, F., Brick, P., Werner, F., Weinzierl, R.O., and Onesti, S. (2001). Structure of an archaeal homolog of the eukaryotic RNA polymerase II RPB4/RPB7 complex. Mol. Cell *8*, 1137–1143.

Tschochner, H. (1996). A novel RNA polymerase I-dependent RNase activity that shortens nascent transcripts from the 3′ end. Proc. Natl. Acad. Sci. USA *93*, 12914–12919.

Van Mullem, V., Landrieux, E., Vandenhaute, J., and Thuriaux, P. (2002). Rpa12p, a conserved RNA polymerase I subunit with two functional domains. Mol. Microbiol. *43*, 1105–1113.

Warner, J.R. (1999). The economics of ribosome biosynthesis in yeast. Trends Biochem. Sci. *24*, 437–440.

Weilbaecher, R.G., Awrey, D.E., Edwards, A.M., and Kane, C.M. (2003). Intrinsic transcript cleavage in yeast RNA polymerase II elongation complexes. J. Biol. Chem. *278*, 24189–24199.

Whitehall, S.K., Bardeleben, C., and Kassavetis, G.A. (1994). Hydrolytic cleavage of nascent RNA in RNA polymerase III ternary transcription complexes. J. Biol. Chem. *269*, 2299–2306.

Wind, M., and Reines, D. (2000). Transcription elongation factor SII. Bioessays *22*, 327–336.

Yamamoto, K., Yamamoto, M., Hanada, K., Nogi, Y., Matsuyama, T., and Muramatsu, M. (2004). Multiple protein-protein interactions by RNA polymerase I-associated factor PAF49 and role of PAF49 in rRNA transcription. Mol. Cell. Biol. *24*, 6338–6349.

Yuan, X., Zhao, J., Zentgraf, H., Hoffmann-Rohrer, U., and Grummt, I. (2002). Multiple interactions between RNA polymerase I, TIF-IA and TAFI subunits regulate preinitiation complex assembly at the ribosomal gene promoter. EMBO Rep. *3*, 1082–1087.

Accession Numbers